The Impact of the Direct Radiative Effect of Increased CO_2 on the West African Monsoon

HARRY MUTTON,[a] ROBIN CHADWICK,[b] MATTHEW COLLINS, F. HUGO LAMBERT,[a] RUTH GEEN,[a] ALEXANDER TODD,[a] AND CHRISTOPHER M. TAYLOR[c]

[a] *University of Exeter, Exeter, United Kingdom*
[b] *Global Systems Institute, University of Exeter and Met Office Hadley Centre, Exeter, United Kingdom*
[c] *Centre for Ecology and Hydrology, Wallingford, United Kingdom*

(Manuscript received 28 April 2021, in final form 4 January 2022)

ABSTRACT: Projections of future West African monsoon (WAM) precipitation change in response to increasing greenhouse gases are uncertain, and an improved understanding of the drivers of WAM precipitation change is needed to help aid model development and better inform adaptation policies in the region. This paper addresses one of those drivers, the direct radiative effect of increased CO_2 (i.e., the impact of increased CO_2 in the absence of SST warming and changes in plant physiology). An atmosphere-only model is used to examine both the equilibrium response and the evolution of the change over the days following the instantaneous CO_2 increase. In response to the direct radiative effect, WAM precipitation increases due to a weakening of the shallow meridional circulation over North Africa, advecting less dry air into the convective column associated with the monsoon. Changes in the shallow circulation are associated with atmospheric and surface warming patterns over North Africa. A large-scale atmospheric warming pattern, whereby North Africa warms more than the monsoon region, leads to a northward shift in the Saharan heat low. In response to increased precipitation in the Sahel, local soil moisture feedbacks play a key role in determining the low-level circulation change and the location of the intertropical discontinuity. The large-scale warming patterns over North Africa result from differing levels of constraint applied by convective quasi-equilibrium. While this constraint acts strongly in the equatorial WAM region, preventing the region from warming in response to the direct radiative effect, North Africa is not strongly constrained and is therefore able to warm.

KEYWORDS: Atmosphere; Africa; Monsoons; Climate change

1. Introduction

The West African monsoon (WAM) is a large-scale atmospheric circulation that is associated with the summer rainy season over West Africa (Akinsanola and Zhou 2020). Changes in the WAM can have particularly large socioeconomic impacts due to the low adaptive capacity of the large population and the dependence on the WAM for sustaining rain-fed agriculture (Akinsanola and Zhou 2020; Cook and Vizy 2019; Raj et al. 2019). With this in mind, the importance of understanding how the WAM is likely to change is clear, particularly in light of a changing climate. Despite this, GCM projections in WAM precipitation remain uncertain with potential for both large increases and decreases (Raj et al. 2019; Wang et al. 2020; Gaetani et al. 2017). The WAM precipitation response to different aspects of the increased CO_2 forcing across eight CMIP6 models (Fig. 1) demonstrates this large spread in projections. It is evident that with such uncertainty in precipitation projections, adaptation policies are likely to be poorly informed. With a large vulnerable population (Raj et al. 2019; Barros et al. 2015; Cook and Vizy 2019) and the potential for substantial changes to the climate, reduced uncertainty in model projections of WAM precipitation should be established. One way this can be achieved is through gaining a better understanding of the factors that drive precipitation change in climate models (Chadwick et al. 2017).

The full forcing of increased CO_2 contains a number of direct and indirect effects that can each influence the WAM [such as the direct radiative effect, or the indirect effects of changing sea surface temperatures (SSTs) or changing plant physiology]. Breaking down the full CO_2 forcing can simplify the response in GCM experiments and can allow the relevant mechanisms driving precipitation change to be identified. Typically this has been performed using atmosphere-only GCM (AGCM) experiments using prescribed SSTs (e.g., Chadwick et al. 2017, 2019; Gaetani et al. 2017). In these experiments the direct radiative effect refers to the impact of quadrupling CO_2 concentrations while keeping SSTs fixed and only allowing the increase in CO_2 to be seen by the radiation scheme (thus causing no change to plant physiology). In this paper the anomalies associated with the direct radiative effect have been calculated using the amip-4xCO2 experiment. The indirect effect of increased CO_2 through changes in SSTs can be isolated using experiments that apply changes to the prescribed SSTs while keeping the concentrations of atmospheric CO_2 constant. In this paper the anomalies associated with a uniform SST warming have been calculated using the amip4K experiment. Across the tropics, it has been shown that the direct radiative effect impacts precipitation through a dynamical weakening of the large-scale circulation, causing precipitation to decrease in regions of climatological ascent and increase in regions of climatological subsidence (Bony et al. 2013; Xia and Huang 2017). The direct radiative effect has also been shown to cause the precipitation to decrease over the ocean and increase over the land whereas a uniform

Corresponding author: Harry Mutton, hm580@exeter.ac.uk

DOI: 10.1175/JCLI-D-21-0340.1

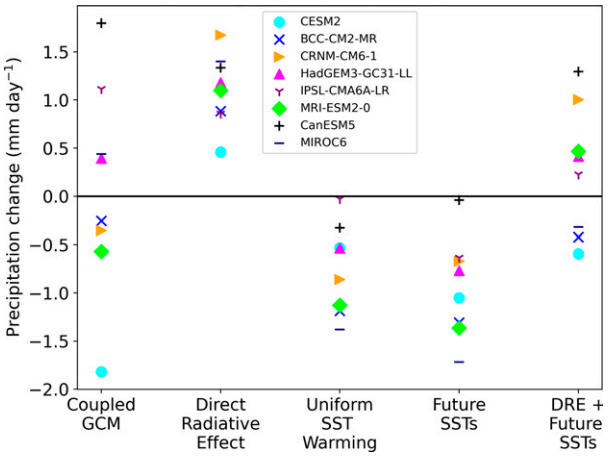

FIG. 1. West African monsoon precipitation response to different forcings in eight CMIP6 GCMs: coupled GCM (Abrupt-4xCO2 − piControl), direct radiative effect (amip-4xCO2 − amip), uniform SST warming (amip-p4K − amip), and future SSTs (amip-future4K − amip). DRE + future SSTs refers to the sum of the direct radiative effect and future SST forcing. WAM precipitation is defined as the area average precipitation over the red box indicated in Fig. 2 between June and August. See text for a description of the different CMIP6 experiments.

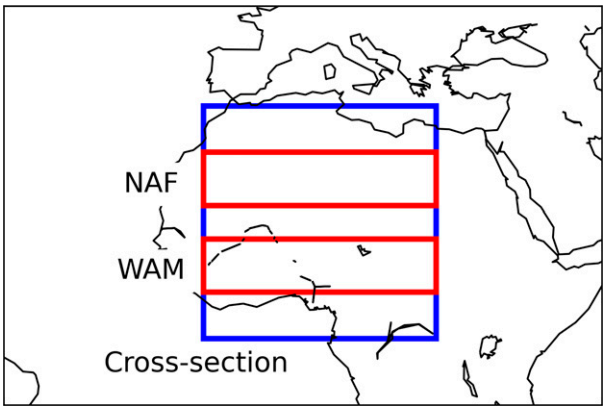

FIG. 2. West African monsoon (WAM), North African (NAF), and zonally averaged cross section areas analyzed.

warming of SSTs tends to increase precipitation over the ocean but decrease over the land (Lambert et al. 2011; Chadwick et al. 2019). Over the WAM region, it has been shown that a uniform SST increase and the direct radiative effect have competing influences on precipitation, with a uniform ocean warming causing a decrease and the direct radiative effect causing an increase (Gaetani et al. 2017; Chadwick et al. 2019). A similar style analysis is shown in Fig. 1, where the impact of different aspects of the increased CO_2 forcing on WAM precipitation in eight different CMIP6 models is presented. Here the WAM precipitation is calculated using a box average across the region indicated in Fig. 2. As expected from previous work, the direct radiative effect causes an increase in precipitation and a uniform SST warming of 4 K causes a decrease. The future SST forcing refers to the impact of a uniform ocean warming with an additional patterned SST change applied; this reflects the projected SST pattern in a future climate under increased CO_2. Comparing the uniform SST warming and future SST columns in Fig. 1, it can be seen that the added pattern in the future SST column does not seem to significantly modify the overall impact of changing SSTs or the spread in projections. It is, however, important to note that the prescribed SSTs in these AGCM experiments are the same for each model. In the coupled models there will be an additional degree of uncertainty stemming from the different SST changes in each model. Chadwick et al. (2017) and Skinner et al. (2012) highlighted that in order to replicate coupled model precipitation change patterns in atmosphere-only models it is necessary to force each AGCM with SST pattern change from the corresponding coupled model. This is not the case in the AMIP-based AGCM experiments used to find the impact of the direct radiative effect or SST changes in Fig. 1, which uses an ensemble mean SST pattern change for all models. This is likely to largely explain why the coupled GCM response in Fig. 1 is not always equal to the sum of the direct radiative effect and the impact of a patterned SST increase. Therefore, the amip4xCO2 and amip4K experiments used in Fig. 1 are still likely to provide useful insight into understanding different mechanisms acting within coupled GCMs and the real world. The combination of effects was found to be relatively linear across several CMIP5 models (Chadwick et al. 2017), although this has not yet been quantified for the CMIP6 models used here.

Figure 3 shows the climatological August temperature and precipitation distribution, and the anomaly caused by the direct radiative effect in an ensemble of eight CMIP6 models. It is shown that climatologically, a precipitation maximum is located at approximately 10°N. In response to the direct radiative effect, this precipitation increases and shifts northward. The climatological distribution of mass-weighted vertically averaged temperature shows a maximum in temperature over the Sahara and the direct radiative effect causes a warming to the north of this climatological maximum.

Despite the increase in WAM precipitation due to the direct radiative effect being a well-established result, the underlying mechanism causing this is poorly understood. Chadwick et al. (2019) demonstrated, using a set of prescribed land experiments, where the land surface temperatures were fixed to present-day (amip) values, that the changes in precipitation and temperature seen in response to the direct radiative effect are still simulated even in the absence of surface temperature changes. This suggests that a simple picture of differential surface warming between dry and moist regions is not sufficient in explaining the simulated changes in precipitation and temperature over northwest Africa. Chadwick et al. (2019) hypothesized that the precipitation increase occurs as a result of enhanced atmospheric warming over the Sahara driving a stronger monsoonal flow. Investigating the cause of this enhanced warming, they suggested that while moist regions can adjust to the radiative heating through a reduction in latent heating, dry regions cannot due to the lack of moisture, and thus the drier desert region warms more. However,

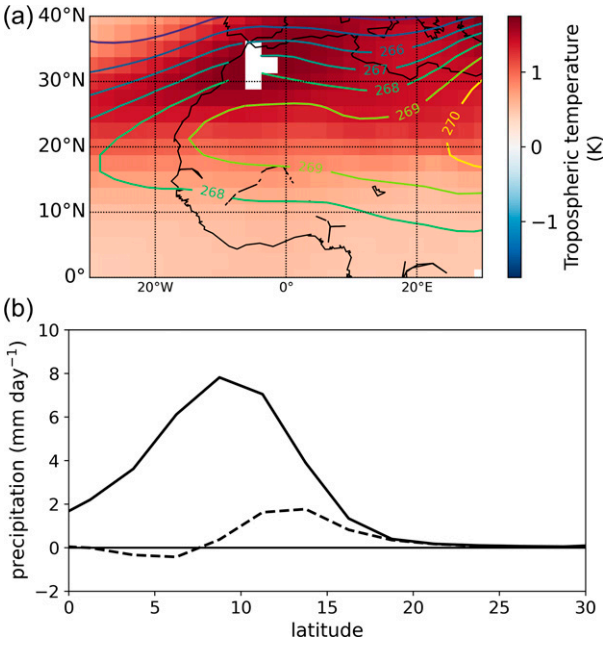

FIG. 3. CMIP6 eight-model ensemble of (a) August mass weighted vertically averaged temperature between 850 and 250 hPa, amip climatology (line contours), and amip-4xCO2 − amip anomaly (colors) (all units in K) and (b) August precipitation zonally averaged between 10°W and 25°E (see cross section indicated in Fig. 2), amip climatology (solid line) and amip-4xCO2 − amip anomaly (dashed line).

both this mechanism for differential warming over Africa and the link between the North African warming and the precipitation increase are yet to be fully investigated. Merlis (2015) investigated differential heating in response to increased CO_2, suggesting that differential heating is caused by cloud and water vapor masking, causing anomalous energy input into the atmosphere to be greater over drier subsidence regions compared to moist convective regions with high cloud. In the absence of circulation changes, this would lead to enhanced warming over the dry subsidence regions and less warming in convective regions (a pattern consistent with Fig. 3).

The underlying mechanism behind the impact of the direct radiative effect of increased CO_2 on the WAM is not fully understood, despite it being a consistent response seen across a range of CMIP6 (and CMIP5) models (Fig. 1), and having been previously discussed by Chadwick et al. (2019) and Gaetani et al. (2017). A single model analysis investigating this mechanism in more depth can help improve understanding of the processes involved. The advantage of a single model analysis is that we are able to make use of experiments and diagnostics that are not part of CMIP6 but which provide valuable additional insights. In this paper the following questions are addressed:

- What is the underlying mechanism behind the precipitation changes resulting from the direct radiative effect?
- What causes the warming patterns seen over North Africa?

It will be shown that the precipitation increase resulting from the direct radiative effect is caused by a reduction in midlevel dry air advection into the monsoon rainband. This results from changes in the shallow meridional circulation responding to warming patterns over North Africa and soil moisture feedbacks. The enhanced warming over North Africa is shown to be enabled by a weaker constraint on atmospheric temperature. In contrast, the WAM region, being an area of convection and closer to the equator compared to North Africa, is constrained to a greater degree by convective quasi-equilibrium (CQE) and the weak temperature gradient (WTG) approximation, preventing the region from warming as much. CQE theory assumes convection happens rapidly and causes the atmosphere to maintain a moist adiabatic lapse rate. This means that in the absence of entrainment, the temperature of the atmosphere will be governed by the temperature and humidity below the cloud base (Emanuel et al. 1994). The WTG approximation assumes that at low latitudes, the Coriolis parameter is small and therefore larger temperature gradients in the free troposphere cannot be maintained (Sobel et al. 2001).

Section 2 discusses the WAM climatology and variability, highlighting the relevant circulations associated with the WAM system. Section 3 describes the model and experiment design used for the analysis and section 4 describes the methods used. Section 5 investigates the equilibrium response to the direct radiative effect analyzing both the increase in WAM precipitation and the northward shift. Section 6 looks into the spinup transition toward the equilibrium response, investigating regional-scale soil moisture feedbacks and larger-scale differential warming patterns. Finally conclusions are given in section 7.

2. WAM climatology and variability

Historically, monsoons have been characterized by a shift in the prevailing wind direction and have been described as large-scale sea breeze systems caused by differing heat capacities between the land and ocean, where the lower surface heat capacity of the land is an important factor in causing the monsoon precipitation to extend farther poleward than the oceanic ITCZ (Zhou and Xie 2018). More recent developments in understanding monsoon dynamics have demonstrated that monsoons can be viewed more accurately as "a localized extreme migration of the tropical convergence zone … pulled poleward over the continent" (Geen et al. 2020, p. 4). The WAM is an example of such a system where the tropical convergence zone progresses from a position over the Gulf of Guinea during spring, inland over the continent during the Northern Hemisphere summer. The onset of the WAM begins near the start of May and reaches its maximum intensity around the middle of August (Cook and Vizy 2019). A schematic depicting the climatological circulation over West Africa during the monsoon season can be seen in Fig. 4. The WAM rainband in August is located at approximately 10°N and is associated with the ascending branch of the Hadley circulation, extending through the depth of the troposphere. A shallow meridional circulation (SMC) extends farther

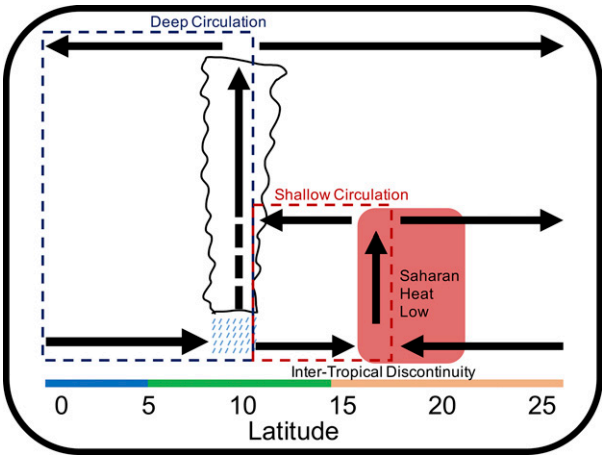

FIG. 4. Schematic depicting the climatological circulation over West Africa during the monsoon season.

poleward across the Sahara, with a southerly low-level flow toward a region of low-level convergence and ascent around 17°N. This region of low-level convergence is known as the intertropical discontinuity and is the boundary between the moist monsoon air mass to the south and the dryer Saharan air-mass to the north. The ascending branch of the SMC extends to approximately 700 hPa where there is horizontal divergence and a return northerly flow toward the monsoon rainband. This shallow circulation is closely related to the Saharan heat low, which is characterized by a region of large low-level atmospheric thickness (LLAT). This causes a region of low pressure and convergence near the surface, and a region of high pressure and divergence at midlevels (Shekhar and Boos 2017).

Variability in the WAM can be caused by a range of factors, such as SSTs in the tropical Atlantic Ocean (Losada et al. 2010) and the Mediterranean (Gaetani et al. 2010), midlatitude synoptic disturbances (Chauvin et al. 2010), and dust emissions (Lavaysse et al. 2011). Even SSTs in the tropical Pacific (Rowell 2001) and the Indian Ocean (Cook and Vizy 2019) have been shown to influence the WAM (Cook and Vizy 2019; Gaetani et al. 2017; Akinsanola and Zhou 2020). This variability is amplified by processes that occur within the region, such as changes in soil moisture or vegetation (Zeng et al. 1999; Giannini et al. 2003). Each of these factors affects the WAM through various pathways, and an increase in precipitation can be ultimately caused by an increase in moisture supplied by the monsoonal flow, a weakening of the SMC that tends to advect dry air into the monsoon rainband at midlevels, or an increase in wind shear that provides more favorable conditions for the organization of mesoscale convective systems (Biasutti 2019).

3. Model and experiment design

An analysis of a single model (HadGEM2-A) forms the basis for the majority of the results presented in this paper. HadGEM2-A has a horizontal resolution of 1.85° longitude × 1.25° latitude and 38 vertical model levels with most variables provided on 17 pressure levels. A more in-depth description of the model configuration and setup can be found in Martin et al. (2011).

The analysis is centered around simulations as used by Todd (2018) involving a set of experiments based on the Atmosphere Model Intercomparison Project (AMIP; the set is referred to herein as the amip experiments). The amip experiments use prescribed SSTs set to observed values between 1979 and 2008, and atmospheric constituents are also set to historical levels. An ensemble of seven start dumps of atmospheric state and soil moisture are obtained from the CMIP5 HadGEM2-A (r1i1p1) amip experiment on 1 August every other year between 1986 and 1998. These start dumps provide the initial conditions for an ensemble of model runs between 1 August 1986 and 30 December 1998. This seven member ensemble is performed for amip and amip-4xCO2 experiments, where amip-4xCO2 has an identical experimental setup to amip but with CO_2 levels multiplied by 4 and this change in CO_2 only seen by the radiation scheme. Comparing the amip and amip-4xCO2 experiments provides an estimate of the equilibrium response to the direct radiative effect.

In addition to this equilibrium response, a set of spinup experiments are used to examine how the system transitions between the amip and amip-4xCO2 equilibrium states. These experiments branch from the seven-member amip ensemble on three occasions (1 August 1988, 1990, and 1997). At these times, CO_2 concentrations are multiplied by 4 and the model is run for 5 months, with daily output of the variables of interest (although here only the first month has been used for the analysis). These spinup experiments are termed amip-4xCO2-spinup. Using the seven ensemble members for each of the three spinup branches, a 21-member ensemble is obtained. These three time periods are also used to analyze the amip and amip-4xCO2 experiments, allowing the different experiments to be compared. This provides a 21-member ensemble of amip, amip-4xCO2, and amip-4xCO2-spinup experiments analyzing the month of August with seven equilibrium runs and three occasions over which the spinup experiment is performed.

Latitude–pressure cross sections of August meridional and vertical winds and precipitation across West Africa, taken from observations, the HadGEM2-A amip experiment, and the anomaly associated with the equilibrium response to the direct radiative effect, are shown in Fig. 5, where a zonal mean has been taken across the blue cross section box in Fig. 2. Comparing circulation and precipitation patterns in HadGEM2-A to those from reanalysis and observational datasets (Figs. 5a,b), it is shown that HadGEM2-A is able to produce a correct circulation pattern, with both shallow and deep circulations extending slightly less poleward compared to the reanalysis. This shallow and deep circulation pattern is also seen in the CMIP6 ensemble (not shown). The precipitation distribution shown in Figs. 5a and 5b also shows consistency between the observations and HadGEM2-A, with the model simulating slightly less rain during August compared to the observations. The precipitation response to the direct radiative effect shown in Fig. 5c demonstrates consistency

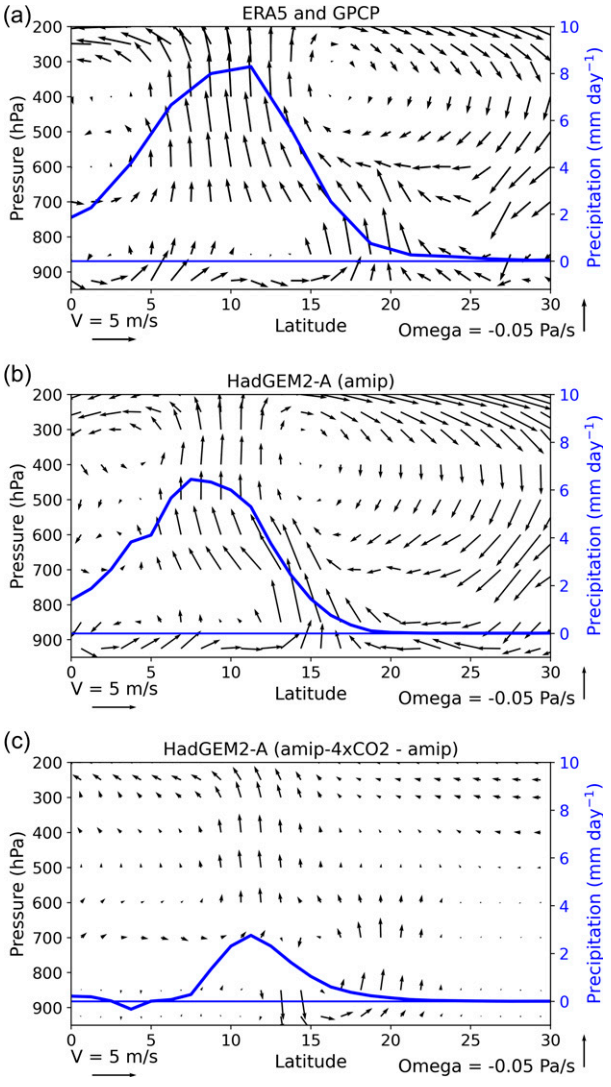

FIG. 5. August meridional circulation (arrows) and precipitation (blue lines), zonally averaged between 10° W and 25°E (see cross section indicated in Fig. 2) from (a) ERA5 and GPCP reanalysis/observations climatology, (b) the HadGEM2-A amip simulation, and (c) the anomalous HadGEM2-A response to the direct radiative effect (i.e., amip-4xCO2 − amip).

between HadGEM2-A and the eight-CMIP6 model ensemble (Fig. 3b), with both an increase and a northward shift in rainfall.

4. Methods

a. Regions

Three regions are used for the analysis, each with a longitudinal range between 10°W and 25°E (Fig. 2):

- The WAM region is characterized averaging between 7° and 15°N, capturing much of the monsoon region defined as the area where the annual range in rainfall exceeds 180 mm and the summer rainfall accounts for over 35% of the total annual rainfall (Wang and Ding 2006).
- The North African (NAF) region is characterized averaging between 20° and 27°N, capturing the regions of maximum tropospheric temperature and LLAT associated with the Saharan heat low (see Figs. 3a and 9).
- zonal mean across the 10°W–25°E longitudinal range has been calculated to produce a latitude–pressure cross section. This is consistent with the region used by Shekhar and Boos (2017) in their analysis of the SMC over West Africa.

b. Definitions of key quantities

The set of equations used to calculate key quantities such as mass-weighted vertical averages, moist static energy (MSE), horizontal divergences, and LLAT can be found in the appendix.

5. Results: Equilibrium response

Based on the precipitation response to the direct radiative effect shown in Figs. 3b and 5c, two aspects of the change, the increase in WAM precipitation and its northward shift, are considered.

a. Increase in WAM precipitation

As mentioned in section 2, an increase in WAM precipitation can generally be caused through an increase in moisture supplied by the monsoonal flow, through a weakening of the SMC, or through changes in wind shear affecting the organization of mesoscale convective systems. Due to the coarse resolution of the climate models analyzed, the GCM response to the direct radiative effect is unlikely to be caused by changes in mesoscale convective systems since these systems will not be resolved (Yang et al. 2019). Therefore in order to understand why we see an increase in precipitation in response to the direct radiative effect, the changes in moisture provided by the monsoonal flow and changes in the SMC are investigated.

An increase in moisture supplied by the monsoonal flow would enhance WAM precipitation through increased MSE or enhanced convergence of winds at the base of the deep convection. To investigate if this occurs in the equilibrium response to the direct radiative effect, a cross section of climatological (amip) and anomalous (amip-4xCO2 − amip) MSE is given in Fig. 6a. Here the latitude of maximum rainfall in the amip experiment is indicated with a vertical dashed black line (8.5°N), the vertical dashed red line shows the latitude of maximum rainfall in the amip-4xCO2 experiment (9.6°N), and the vertical black dotted line shows the location of the ascending branch of the shallow circulation (14.7°N). Climatologically the maximum in low-level MSE lies just north of the monsoon rainband. From Fig. 6a it is shown that there is no large increase in MSE at the base of the deep convection, and at that latitude, any increase in MSE that does exist occurs at mid- to upper levels. This suggests that changes in MSE in the monsoon rainband may be caused by a weakening SMC, advecting less dry air into the region, rather than an increase in moisture supplied by the monsoonal flow at low levels.

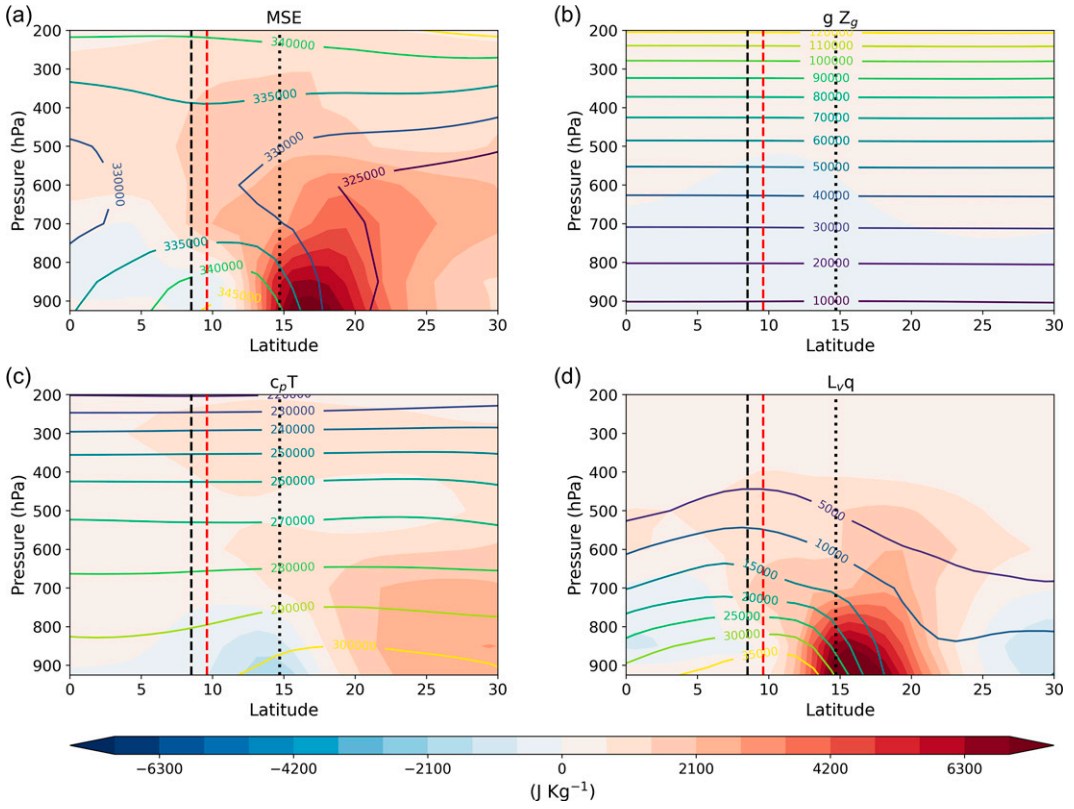

FIG. 6. August cross section of amip climatological (line contours) and amip-4xCO2 − amip anomalous (colors) (a) MSE, (b) gZ_g, (c) C_pT, and (d) L_vq (all units in J kg^{-1}). The location of the monsoon rainband in the amip experiment is indicated with a vertical dashed black line (8.5°N), the vertical dashed red line shows the location of the monsoon rainband in the amip-4xCO2 experiment (9.6°N), and the vertical black dotted line shows the location of the ascending branch of the shallow circulation (14.7°N).

A large increase in MSE is also evident just north of the climatological location of the ascending branch of the SMC. Decomposing the MSE into the individual L_vq and c_pT components [see Eq. (A2)], it is shown that changes in moisture dominate the MSE response. It is noted that the large low-level anomaly in MSE can be thought of more accurately as a northward shift in the intertropical discontinuity. Since SSTs are not warming, the moisture in each air mass is unlikely to change much (Chadwick et al. 2016), meaning changes in moisture are likely to be dynamically driven rather than thermodynamically driven (i.e., changes in moisture are caused by shifts in the position of the intertropical discontinuity rather than a large-scale moistening or drying of an air mass). The cross section of c_pT demonstrates a warming over North Africa and a cooling at low levels between 10° and 20°N.

To investigate further the changes in the SMC, a cross section of horizontal divergence of moisture transport in HadGEM2 is presented in Fig. 7a. Climatologically, regions of low-level convergence and midlevel divergence in horizontal moisture transport are associated with the ascending branch of the SMC. In response to the direct radiative effect, both regions of low-level convergence and midlevel divergence shift northward, indicating a northward shift in the SMC. A 22% reduction in divergence of moisture flux at 700 hPa averaged between 10° and 25°N is calculated, consistent with a reduction in dry air advection into the deep convective cell and conducive to an increase in WAM precipitation. It has also been shown that these changes are dynamically driven rather than thermodynamically (Figs. 7c,e), indicating that it is a weakening in circulation that is causing this response rather than a change in the moisture. This analysis has also been performed looking at the ensemble of eight CMIP6 models (Figs. 7b,d,f). Again, a reduced divergence of moisture flux at midlevels in the monsoon rainband is demonstrated (10%).

To show how the shallow circulation itself changes and how it relates to the deep circulation, divergence of winds at 925, 700, and 200 hPa are shown in Fig. 8. Climatologically the 925-hPa convergence and 700-hPa divergence associated with the shallow circulation can be seen around 14°–17°N and in response to the direct radiative effect, both these features weaken and shift northward. Again at 700-hPa averaging between 10° and 25°N, a 36% reduction in the divergence of winds is calculated for HadGEM2 (indicated by the gray shaded area in Fig. 8b), and 21% for the CMIP6 model ensemble. The divergence at 200 hPa is associated with the deep circulation, and in response to the direct radiative

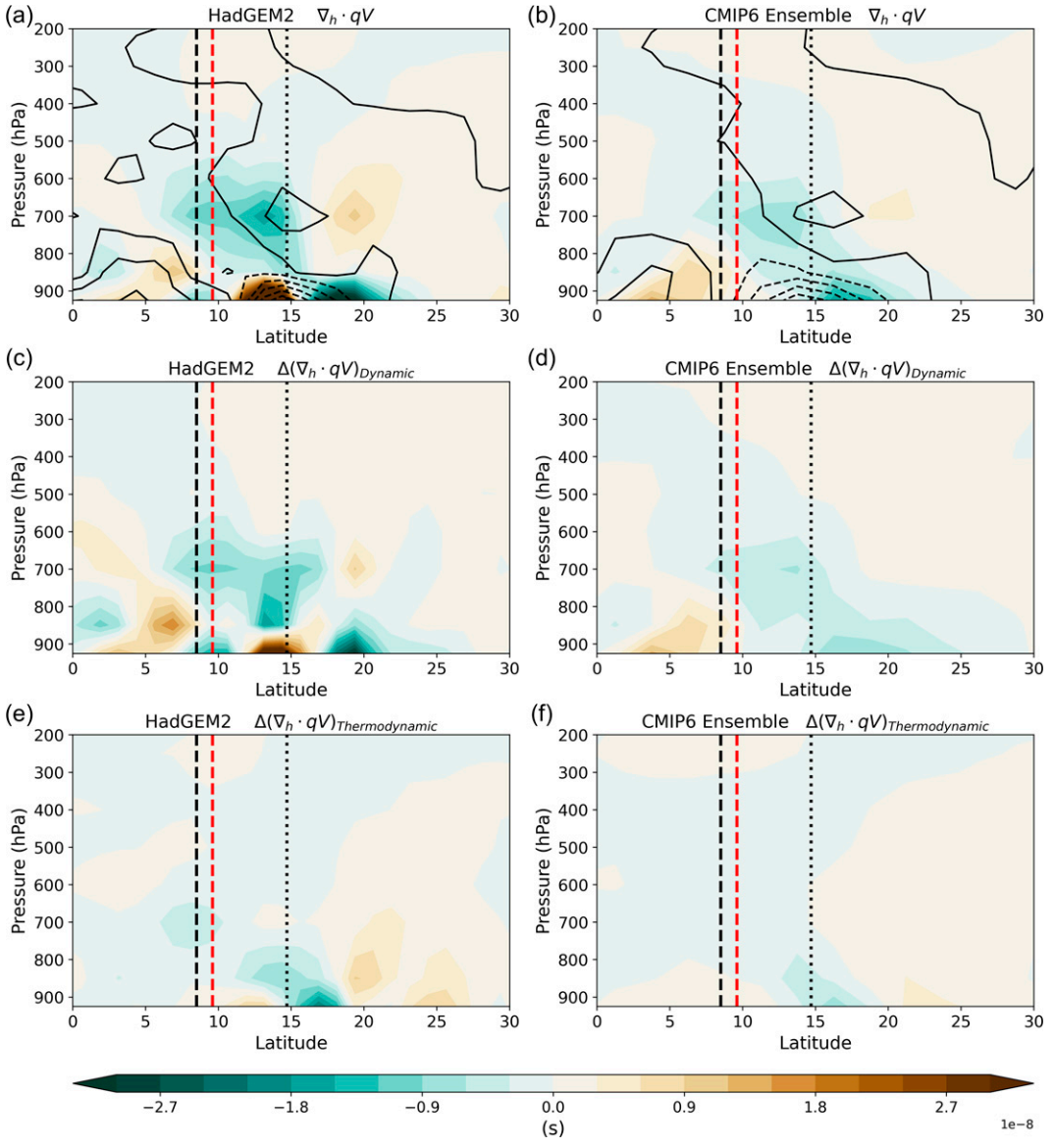

FIG. 7. August cross section of (left) HadGEM2 and (right) eight CMIP6 model ensemble. (a),(b) The amip climatological (black line contours), and amip-4xCO2 − amip anomalous (colors) horizontal divergence of moisture transport, $\nabla_h \cdot q\mathbf{V}$ (s^{-1}). Dashed black lines indicate negative values (convergence), and solid black lines indicate positive values (divergence). (c),(d) Dynamic component of amip-4xCO2 − amip anomalous horizontal divergence of moisture transport, $\nabla_h \cdot (q_A \Delta \mathbf{V})$. (e),(f) Thermodynamic component of amip-4xCO2 − amip anomalous horizontal divergence of moisture transport, $\nabla_h \cdot (\mathbf{V}_A \Delta q)$. As in Fig. 6, the location of the monsoon rainband in the amip experiment is indicated with a vertical dashed black line (8.5°N), the vertical dashed red line shows the location of the monsoon rainband in the amip-4xCO2 experiment (9.6°N), and the vertical black dotted line shows the location of the ascending branch of the shallow circulation (14.7°N).

effect, this divergence strengthens, consistent with enhanced precipitation.

Since the SMC is directly related to the Saharan heat low, changes in LLAT are also investigated (Fig. 9). Here, a climatological maximum in LLAT is seen over the central Sahara. The anomaly caused by the direct radiative effect demonstrates an increase in LLAT to the north of this climatological maximum. This is consistent with the response in mass-weighted vertically averaged temperature presented in Fig. 3, highlighting the fact that temperature and atmospheric thickness are very closely related. This demonstrates how changes in temperature over North Africa affect the Saharan heat low and thus impact the SMC. Shekhar and Boos (2017) demonstrated using a reanalysis dataset that, under interannual variability, a northward shift in the Saharan heat low is related to a weakened shallow circulation. This is a signal that is evident in the reduction in

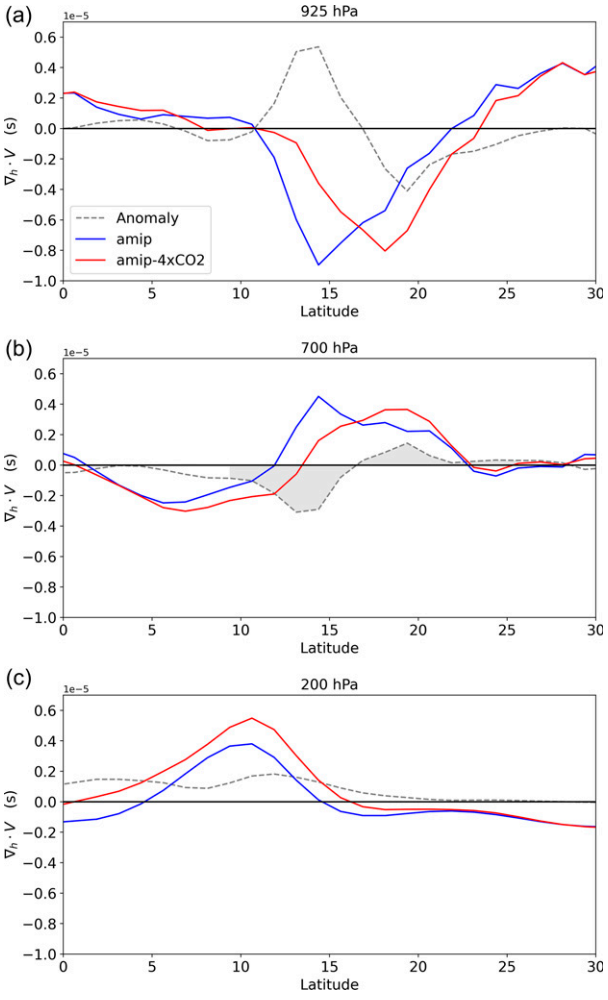

FIG. 8. August HadGEM2 horizontal divergence of winds, $\nabla_h \cdot \mathbf{V}$ (s^{-1}), zonally averaged between 10°W and 25°E at (a) 925, (b) 700, and (c) 200 hPa. Gray shaded area in (b) indicates the region averaged over to calculate percentage change in shallow circulation strength.

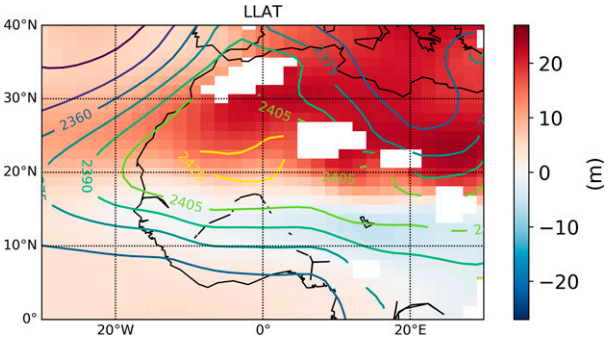

FIG. 9. August amip climatology (line contours) and amip-4xCO2 − amip anomalous (colors) low-level atmospheric thickness (LLAT; m). Areas of white are caused by topography masking the data.

midlevel (700 hPa) divergence of moisture transport shown in Fig. 7a and the divergence of winds shown in Fig. 8.

In summary, the direct radiative effect causes changes in temperature over North Africa. This leads to a northward shift in the Saharan heat low and SMC. Reduced midlevel divergence resulting from changes in the SMC advects less dry air into the monsoon rainband at midlevels and causes an increase in monsoon precipitation. In section 6 the causes of these changes in temperature are investigated by analyzing the large-scale warming patterns and the more localized impact of soil moisture feedbacks affecting surface heat fluxes.

b. Northward shift in WAM precipitation

The previous section addressed the mechanism leading to an increase in WAM precipitation. However, the precipitation response to the direct radiative effect demonstrates not only an increase but also a northward shift. As previously stated, climatologically, the monsoon rainband lies just equatorward of the low-level MSE maximum (Privé and Plumb 2007; Nie et al. 2010). Shekhar and Boos (2016) demonstrate that integrating MSE between 20 hPa above the surface to 500 hPa provides a good metric for the location of the monsoon rainband, again with the rainband located just equatorward of the MSE maximum. Integrating through this depth is preferred to other more surface based estimations since it accounts for the effect of entrainment into the rainband at midlevels. Here a similar method is used and the MSE has been integrated between 925 and 500 hPa (Fig. 10). As expected, the precipitation maximum lies just equatorward of the MSE maximum, and in response to the direct radiative effect, the maximum in MSE and precipitation both increase and shift northward.

Decomposing this integrated MSE into the individual pressure levels and showing the change in surface MSE (Fig. 11), it is possible to identify which levels of the atmosphere are responsible for both the increase and northward shift in MSE maximum. This decomposition is made clearer in Figs. 11f and 11g where the magnitude of the increase and latitudinal shift in MSE maximum is indicated for each level. The

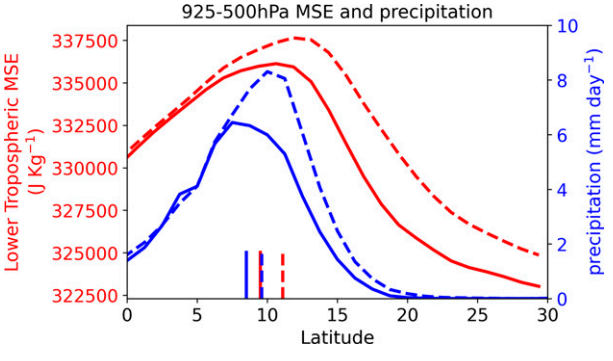

FIG. 10. August amip (solid lines) and amip-4xCO2 (dashed lines) mass weighted vertically averaged MSE between 925 and 500 hPa (red lines) and precipitation (blue lines), zonally averaged between 10°W and 25°E. Vertical dashed lines show the latitude of the maximum in MSE or precipitation.

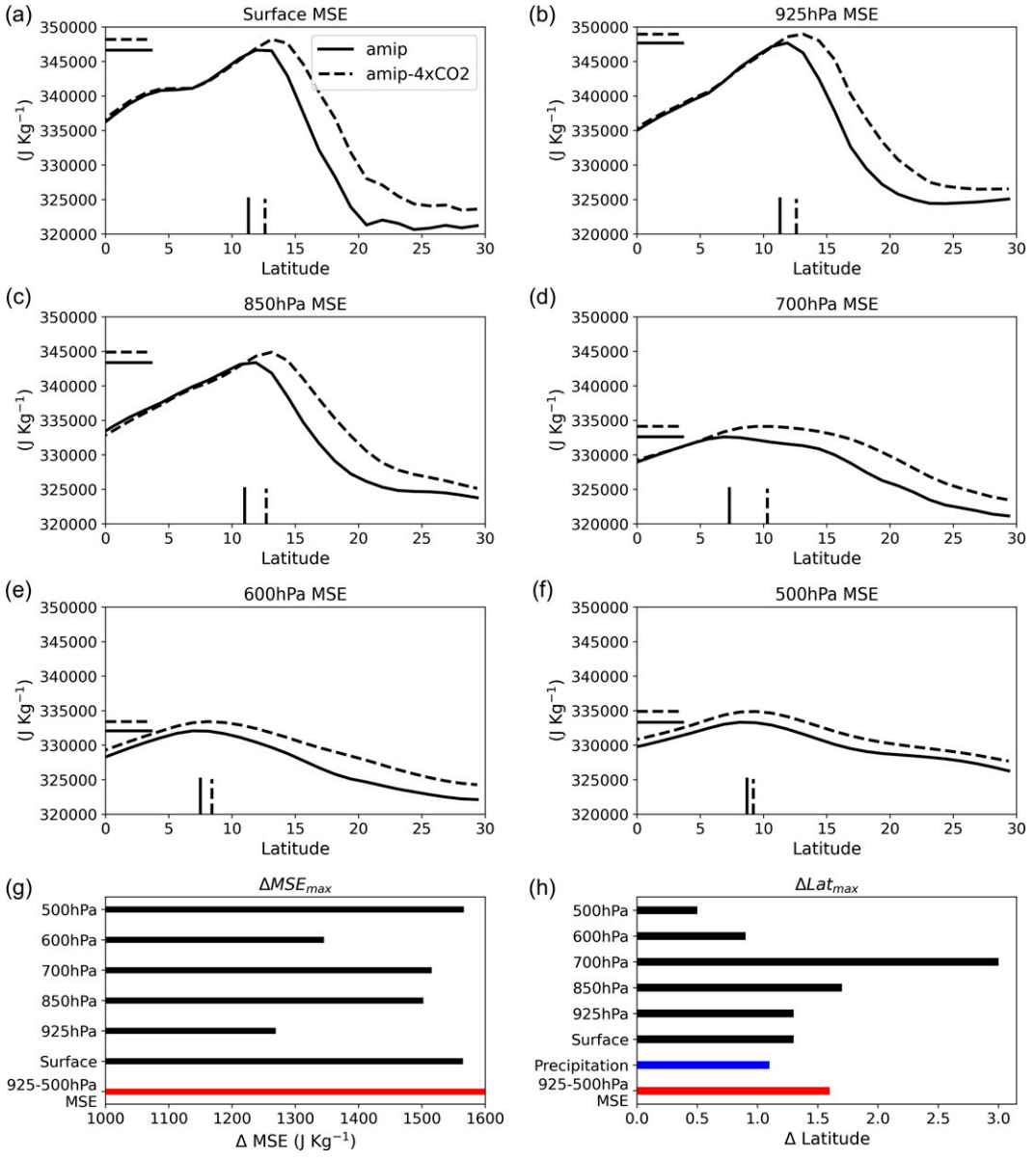

FIG. 11. (a)–(f) August amip (solid lines) and amip-4xCO2 (dashed lines) MSE at the surface, 925, 850, 700, 600, and 500 hPa respectively; vertical and horizontal lines highlight the latitude and magnitude of the MSE maximum at each level. (g) Change in magnitude of MSE maximum between amip and amip-4xCO2 at each level and in vertically averaged MSE. (h) Latitudinal shift in MSE maximum at each level and in vertically averaged MSE and precipitation (shown in Fig. 10) between amip and amip-4xCO2.

increase in magnitude in MSE maximum is seen at all levels, although it is larger at the mid- to upper levels compared to the lower levels. This highlights the role that a reduction in midlevel dry air advection and a weakened shallow circulation has on the MSE increase. The northward shift in MSE is also seen at all levels with a particularly large shift at 700 hPa due to a poorly defined climatological maximum. Here the key message is that the northward shift in the MSE maximum occurs at the surface too and therefore the northward shift in the full integral is not solely due to the effect of changes in dry air advection, but the whole monsoon system shifting northward.

6. Results: Spinup response

Section 5 demonstrated an equilibrium state in which WAM precipitation increased as a result of reduced dry air advection into the monsoon rainband at midlevels, caused by changes in the SMC. Here, the cause of this circulation change is investigated, and since the SMC is a thermally driven

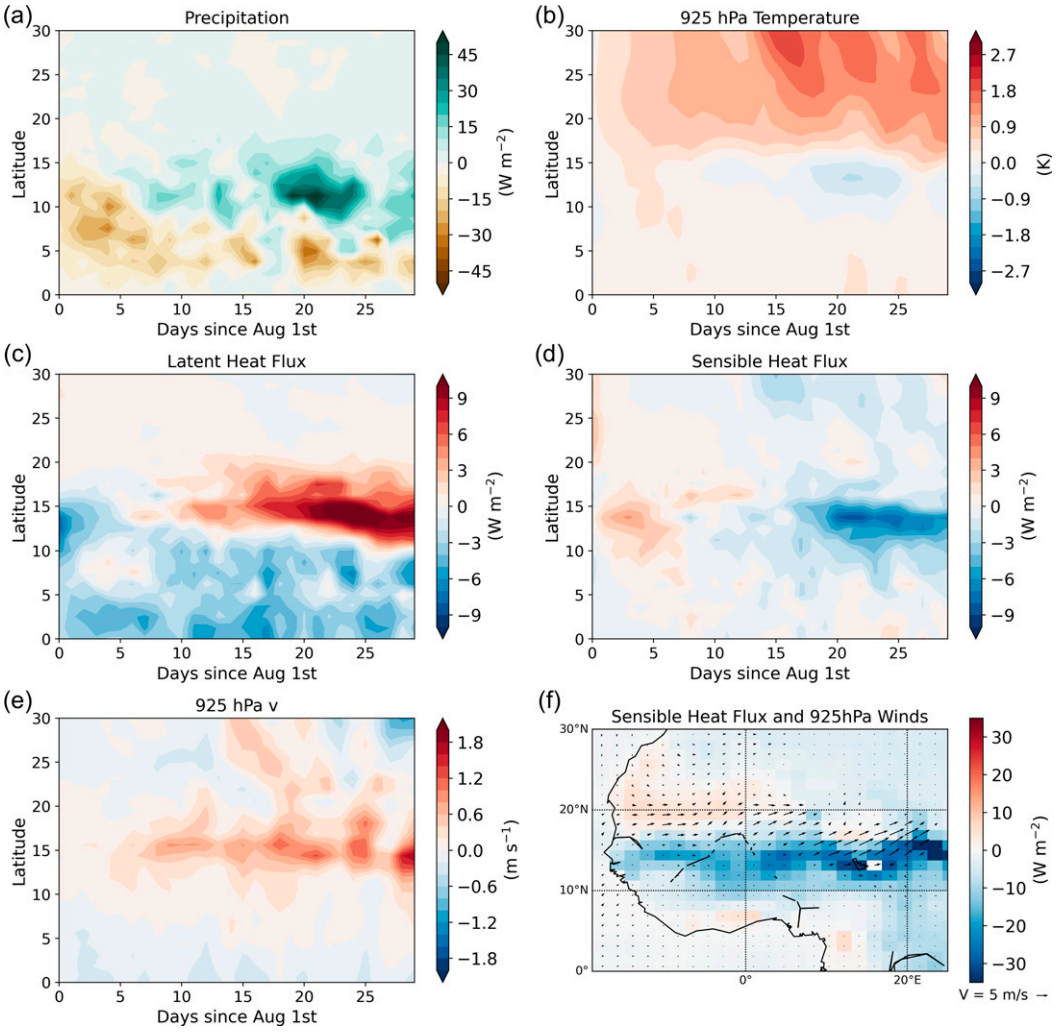

FIG. 12. Time–latitude plots of amip-4xCO2-spinup − amip anomalous (a) precipitation, (b) 925-hPa temperature, (c) surface latent heat flux, (d) surface sensible heat flux, and (e) meridional winds, averaged zonally across the 10°W–25°E cross section. (f) The amip-4xCO2 − amip (equilibrium) anomalous surface sensible heat flux (colors) and 925-hPa winds (arrows).

circulation associated with the Saharan heat low, processes that lead to temperature changes over North Africa are analyzed.

a. Spinup transition to the 4xCO2 state

The amip-4xCO2-spinup experiment is used to investigate how the temperature, precipitation, circulation, and surface heat fluxes change during the 30 days following the CO_2 increase. This provides insight into how the system transitions from the amip to the amip-4xCO2 equilibrium states, and indicates which processes are driving the changes. Time–latitude plots of the variables mentioned are shown in Fig. 12, where for each day a zonal mean across the 10°W–25°E cross section is calculated.

The immediate response to the increase in CO_2 (seen on day 0 of the experiment) is a widespread decrease in precipitation across the whole monsoon region, likely due to an abrupt increase in atmospheric stability. Enhanced warming over North Africa compared to the monsoon region is also evident from day 0 and this is a feature that is discussed further in section 6b.

The surface heat fluxes in the Sahel (a semiarid region between approximately 13° and 17°N) are particularly sensitive to changes in precipitation over the previous days (Lohou et al. 2014). Due to the sparse vegetation cover in the region, during the days following rainfall, evaporation directly from the soil surface is large and the surface sensible heat flux is suppressed. Similarly, in a dry spell, bare soil evaporation is reduced and the sensible heat flux increases. Since plants can access moisture from below the soil surface, transpiration is less variable day to day. Therefore, in the more vegetated regions (south of the Sahel), the surface heat fluxes are less sensitive to rainfall variation. It is evident from Fig. 12 that at Sahelian latitudes, negative precipitation anomalies are

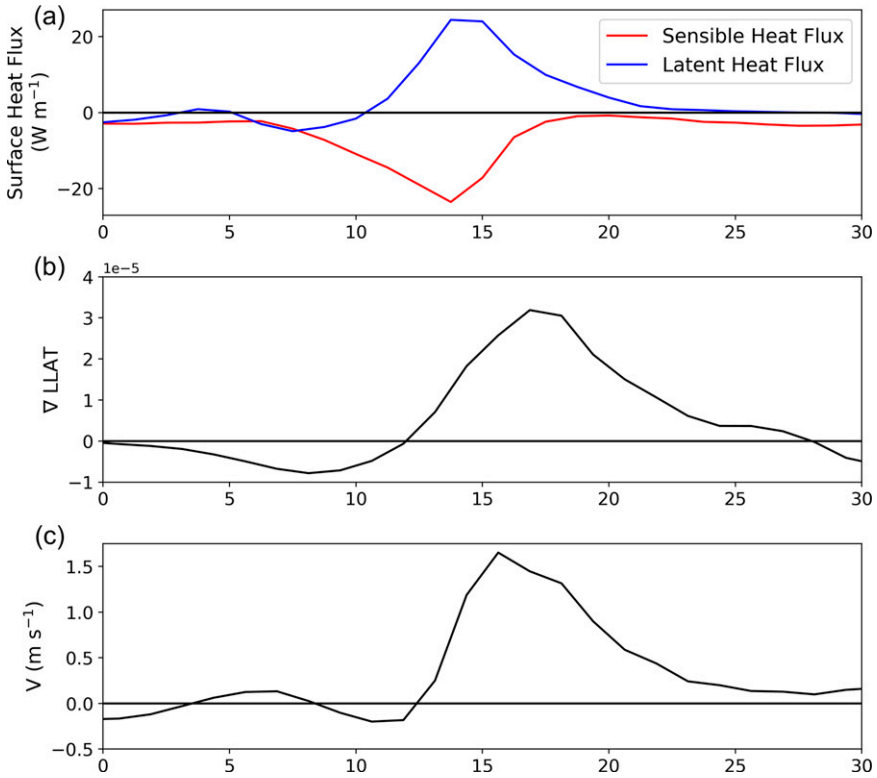

FIG. 13. August amip-4xCO2 − amip anomalous (a) sensible (red) and latent (blue) surface heat fluxes, (b) meridional LLAT gradient, and (c) meridional winds, averaged between 10°W and 25°E.

coincident with a decrease in latent heat flux and an increase in sensible heat flux. This increase in sensible heat flux is responsible for the warm temperature anomaly around days 3–7 between 13° and 17°N.

Throughout the spinup experiment, warming over North Africa is greater than warming over the monsoon region. After the initial precipitation decrease, this large-scale warming pattern acts to shift the precipitation band farther north, a signal that can be seen from day 6 and onward. This precipitation increase causes the latent heat flux to increase and the sensible heat flux to decrease, cooling the atmosphere and reinforcing the large-scale changes in temperature gradient that are forming. The winds over the Sahel respond to changes in this temperature gradient and in the case of the spinup experiment, the changes in temperature, driven by surface heat flux anomalies superimposed onto the large-scale warming pattern, result in a strengthening of the southerly winds. From day 15 onward, the wetter conditions in the Sahel lead to a sustained increase in latent heat flux and a decrease in sensible heat flux. The soil moisture feedback appears to play a key role in determining the location of the intertropical discontinuity and the northward shift in the SMC seen in the equilibrium response. A map of anomalous surface sensible heat flux and anomalous 925-hPa winds from the equilibrium experiment (Fig. 12f) demonstrates that the largest wind anomalies are positioned just north of the decrease in sensible heat flux. The changes in sensible heat flux thus act to locally enhance the low-level meridional temperature gradient and thereby provide a control on the location of the circulation response. These results are consistent with the mechanism leading to a precipitation increase discussed in section 5a.

Plots of anomalous surface heat fluxes, the meridional gradient in LLAT, and 925-hPa meridional wind anomalies in the equilibrium experiment (Fig. 13) help demonstrate the way in which circulation responses are tied to the position of this surface heat flux feedback. Increased latent heat flux in the Sahel region is collocated with a decrease in sensible heat flux. These surface heat flux changes lie just south of an increase in LLAT gradient that is collocated with the increase in meridional winds.

b. Large-scale warming patterns

In section 5a, it is shown that the WAM precipitation increases due to a reduced amount of dry air advection into the monsoon rainband at midlevels resulting from a northward shift and a weakening of the SMC. These changes in circulation are driven by warming patterns caused by the local effect of surface heat flux anomalies over the Sahel, superimposed onto a large-scale warming pattern where North Africa warms more than the monsoon region. This section aims to investigate the cause of this enhanced warming over North Africa.

Again, the amip-4xCO2-spinup experiment is used to investigate how the temperature anomalies form over the month following the increase in CO_2 (Fig. 14b). Over this period, the warming in the NAF region is significantly larger than in the

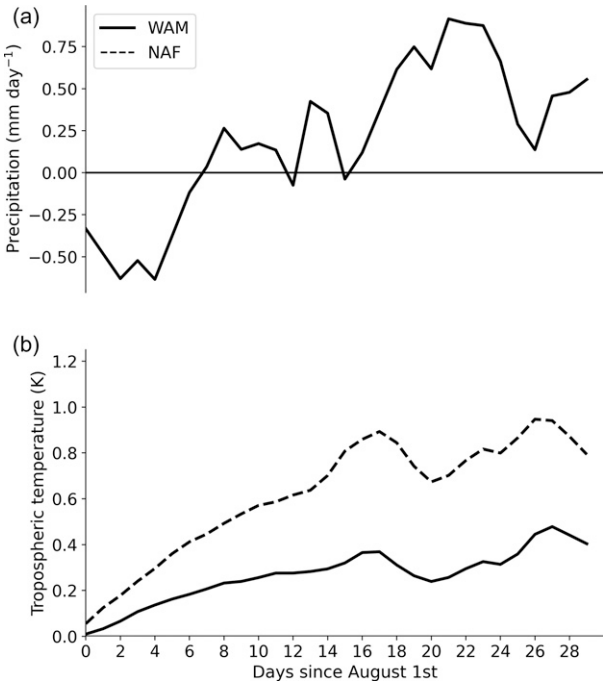

FIG. 14. Time series of amip-4xCO2-spinup − amip anomalous (a) precipitation and (b) mass-weighted vertically averaged temperature over the WAM (solid) and NAF (dashed) regions from the spinup simulations. NAF precipitation is not indicated since both values of climatological and anomalous precipitation in that region are very small.

WAM region, with a p value of less than 0.001 (calculated comparing the trend in temperature in the two regions over the first 17 days of the experiment in each ensemble member). As addressed in section 6a, it is noted that the warming occurs from day 1 of the spinup experiment, whereas the precipitation time series (Fig. 14a) indicates an initial decrease in WAM precipitation. It is not until around day 16 that a substantially positive precipitation anomaly begins to form. This result helps confirm that if a link between the precipitation and the large-scale Saharan temperature anomaly exists, then the temperature anomaly is likely to be causing the precipitation increase rather than the other way round.

To identify the processes driving the different levels of warming over the WAM and NAF regions, the change in temperature has been decomposed into different temperature tendency increments (Figs. 15a,b). Here only the first 17 days of the spinup experiment have been analyzed since this is the timeframe over which the majority of the warming occurs. In the WAM region, since it is a region of convection, the changes in temperature are predominantly caused by changes in convective, advective, and radiative warming. Consistent with the findings of Muller and O'Gorman (2011), the convective temperature increment mirrors the advective temperature changes. The warming due to radiation is positive throughout, associated with the increased levels of CO_2. Over the NAF region, being a dry desert region, the changes in convective warming are small. Instead, the changes in temperature are caused by a reduction in radiative cooling and advective heating. To understand why differing levels of total warming are seen between the WAM and NAF regions, the differences between the WAM and NAF temperature tendency increments have been calculated and compared to the difference in total temperature tendency between the two regions (Figs. 15c–f). If the differential warming between the two regions occurred solely as a result of cloud and water vapor masking, then the total temperature increment would be expected to be well correlated with the radiation temperature tendency increment. However, this is not the case. If Chadwick et al.'s (2019) hypothesis for differential warming across West Africa were true, then the total temperature tendency increment would be expected to be well correlated with the sum of the convection and radiation terms. Again, this is not true. It is found that it is not possible to attribute the differential warming to just one process, and the correlations between the difference in increments and the difference in total warming are weak for each term. These results suggest that the differential warming occurs due to a balance between a number of different terms.

In light of these results, it is suggested that the differential warming between the WAM and NAF regions is driven by differing levels of constraint on atmospheric temperatures. The WAM region, being a convective region close to the equator, is strongly constrained by CQE theory and the WTG approximation. In addition to this, changes in low-level temperature and humidity in the WAM region are small (Fig. 6), possibly due to SSTs remaining unchanged between the amip and amip-4xCO2 experiment and the monsoon inflow at low levels originating over the ocean. CQE theory suggests that in regions of active deep convection (such as the WAM region), the temperature of a column is set by the MSE below the cloud base (Emanuel et al. 1994). Therefore, any free tropospheric warming that occurs in such regions will be caused by changes in MSE below the cloud base (neglecting the changes in entrainment). Since the low-level changes in temperature and humidity are small in the WAM region (Fig. 6), the warming in the rest of the column is constrained to be small too. The WTG approximation could also apply constraints to the temperature in the WAM region. This approximation suggests that free tropospheric temperature gradients in low-latitude regions (where the Coriolis force is weak) are small (Sobel et al. 2001). Therefore, the gradient in temperature change should also be small in order to maintain this WTG. Since the WAM region is close to the equator, the WTG would constrain the region to warm at a similar rate to the rest of the tropics. In contrast, the NAF region is not a convective region and is farther from the equator compared to the WAM region. Therefore, the constraints applied by CQE theory and the WTG approximation will be weaker, enabling the region to warm more. To demonstrate this, scatterplots of temperature tendency due to model physics against temperature tendency due to advection have been produced for each region (Figs. 16a,b). In the WAM region, the two terms are strongly anticorrelated, suggesting that the advection term responds effectively and efficiently to any warming or cooling that occurs from the model physics and vice versa. In contrast, the NAF region does not demonstrate this strong anticorrelation and the two terms are not as well correlated. This

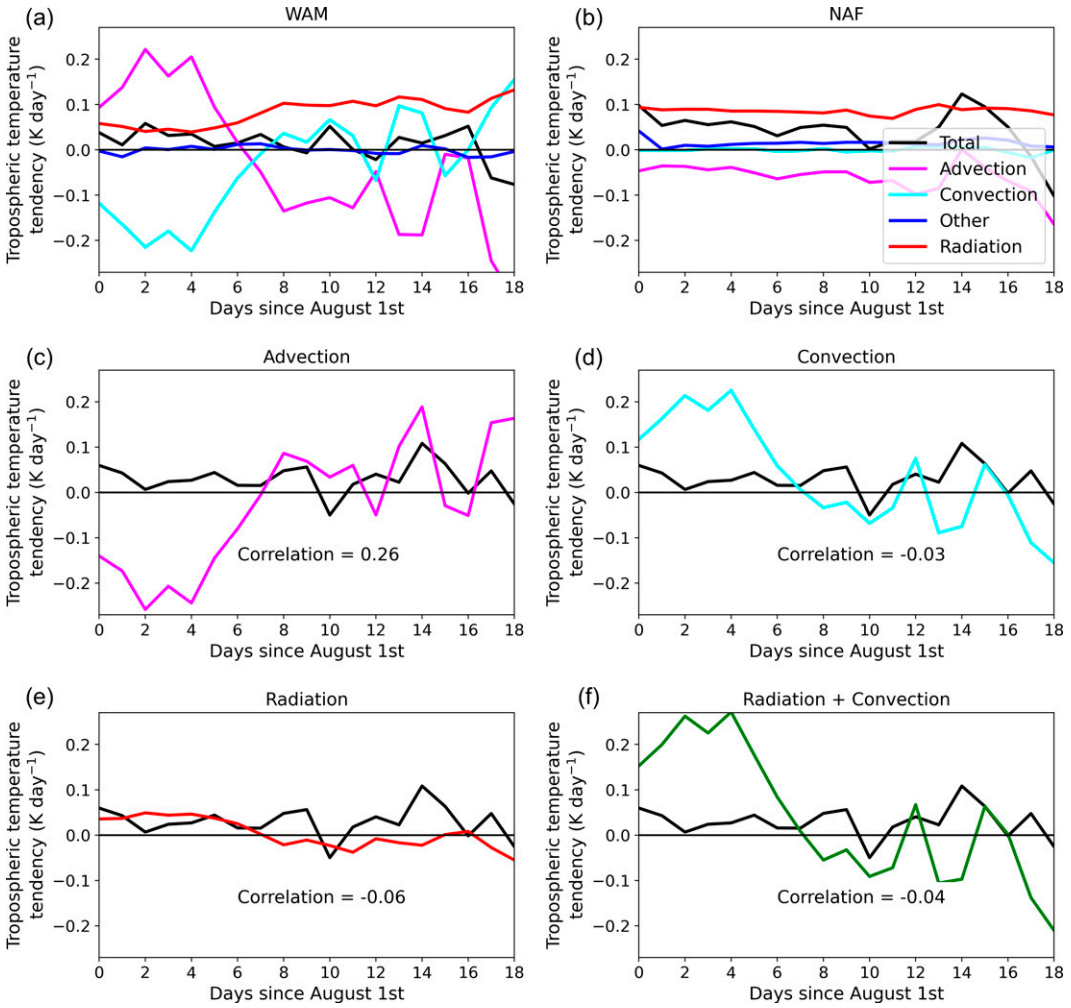

FIG. 15. (a),(b) Time series of amip-4xCO2-spinup − amip anomalous vertically averaged temperature tendency increments between 925 and 250 hPa over the (a) WAM and (b) NAF regions from the spinup simulations. "Other" refers to the sum of boundary layer processes, stratiform precipitation, diffusion, and energy correction, all of which are generally small. Also shown are time series of the difference in WAM and NAF anomalous vertically averaged temperature tendency due to (c) convection, (d) advection, (e) radiation, and (f) the sum of radiation and convection. In each time series, the difference between the WAM and NAF total temperature tendency is shown in a black line and the correlation coefficient between the difference in total temperature tendency and each increment is indicated.

suggests that the advection and model physics terms do not respond quickly to balance one another in this region, and there is net warming driven by increased radiative heating (see Fig. 15b). The strong anticorrelation in the WAM region indicates that the temperature is constrained, whereas the weak correlation in the NAF region indicates a lack of constraint on temperature. Extending this analysis to generalize for all tropical ascent and descent regions between 0° and 30°N, this relationship is still seen, with strong negative correlation between the model physics and advective terms in the ascending regions, and a weak correlation over the descent regions (Figs. 16c,d). This supports the hypothesis that the column temperature in convective regions is more highly constrained than in nonconvective regions in response to the direct radiative effect of increased CO_2.

The above hypothesis relies partly on the changes in low-level temperature and humidity in the WAM region being small. Chadwick et al. (2016) and Byrne and O'Gorman (2016) demonstrate that changes in surface specific humidity over land can be determined by scaling present-day values by the fractional change in surface specific humidity over the oceans. In the amip-4xCO2 experiment, the SSTs remain unchanged compared to the amip experiment, and therefore changes in land specific humidity at the surface should be small. To understand why low-level temperature changes are also small in the WAM region, vertical profiles of total temperature tendency over the first 17 days of the spinup run are shown in Fig. 17. This vertical profile indicates that the warming in the WAM region is largest at midlevels and is small near the surface. Decomposing this into different temperature

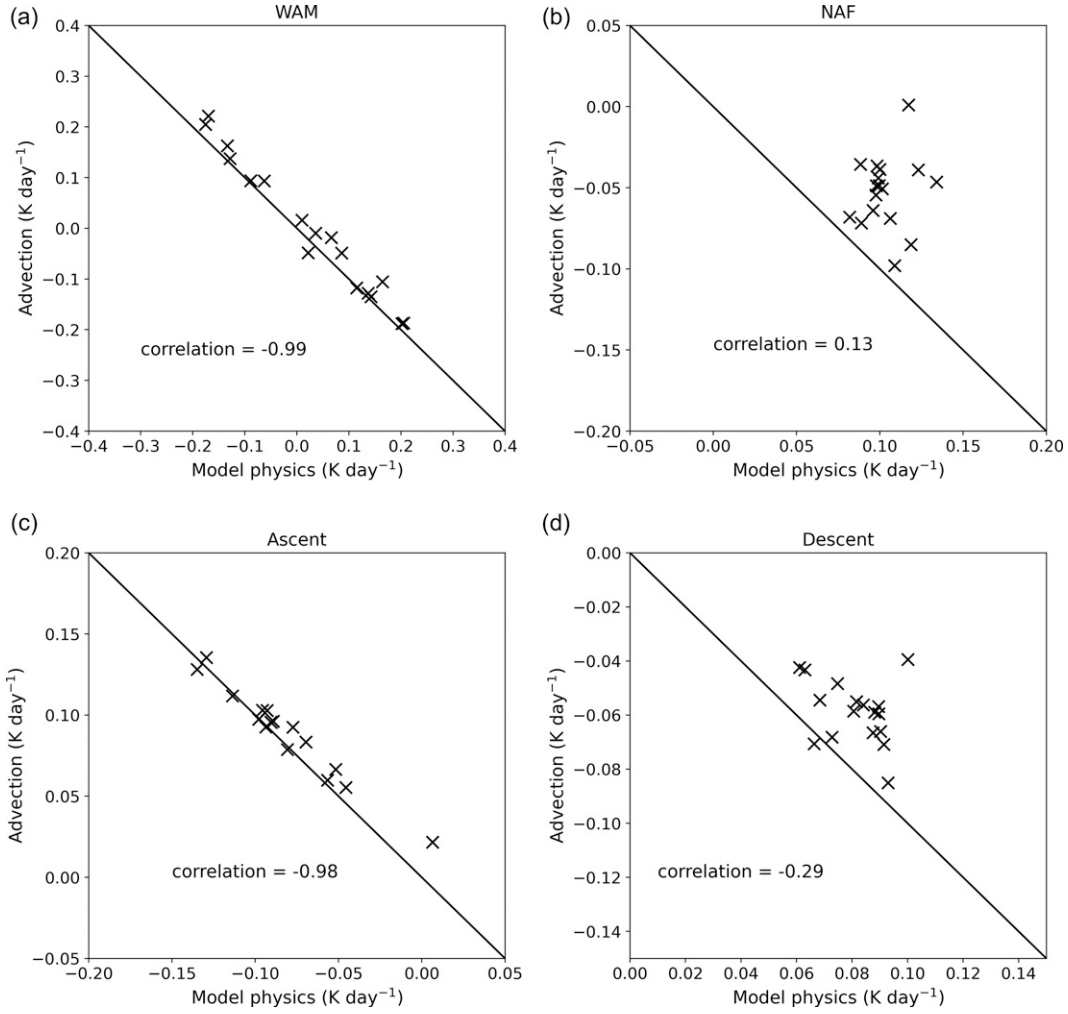

FIG. 16. Scatterplots of mass weighted vertically averaged temperature tendency due to model physics against temperature tendency due to advection for the first 17 days of the spinup experiment over (a) the WAM, (b) the NAF, (c) all regions of ascent (defined as a region where omega is negative) between 0° and 30°N, and (d) all regions of stronger descent (defined as a region where omega is greater than 0.015 m s^{-1}) between 0° and 30°N.

tendency increments, it is shown that this small level of warming occurs due to a changing balance between a number of terms (Fig. 17b). Initially the radiative warming is small near the surface and reaches a maximum at midlevels. Later in the spinup experiment, the radiative warming at low levels increases; however, the total temperature increment is still small, since other terms have acted to balance the changes in radiative warming. It is suggested that, similarly to the lack of subcloud moisture increase in the WAM region, the lack of subcloud temperature increase may also be largely due to the absence of SST warming, which limits the temperature of the monsoon air mass (since it originates over the ocean). However, we do not explore this in more depth here.

To conclude the analysis, it is noted that eventually the advection term must balance the other tendency terms in the NAF region. Analyzing the equilibrium response to the direct radiative effect it is found that the reduced radiative cooling of the NAF region is balanced by a reduction in advective heating. Climatologically, the large-scale circulation advects air at high levels into the NAF region. This air descends and warms, causing the climatological advective heating. In response to the direct radiative effect, this circulation weakens (see Fig. 5c, where climatological descent over latitudes greater than 20°N is reduced) and causes the advective warming associated with the climatological subsidence to reduce. We suggest that the NAF region must warm first in order to weaken this large-scale circulation.

7. Summary and conclusions

Changes in WAM precipitation can have substantial socioeconomic impacts due to the dependence of a large population with low adaptive capacity on the rain that it brings for sustaining rain-fed agriculture. Despite this, projections in WAM precipitation from GCMs are largely uncertain, meaning adaptation policies are likely to be

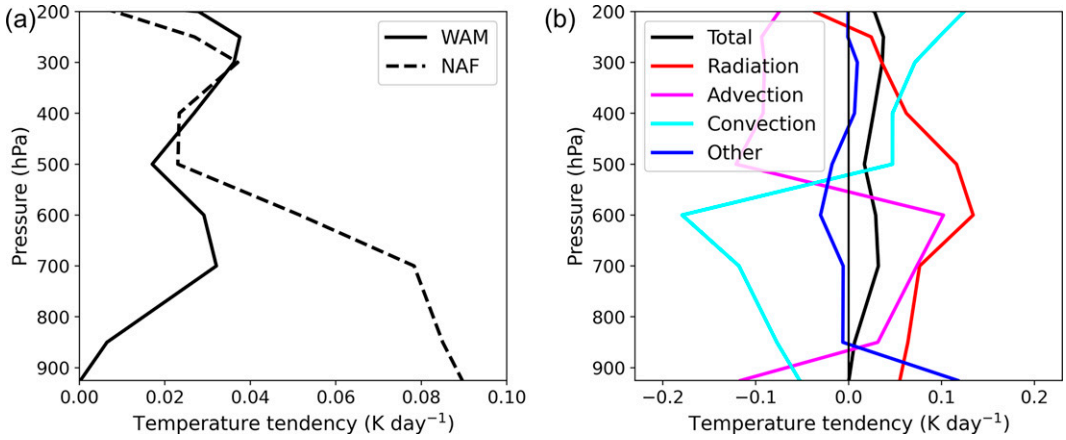

FIG. 17. (a) Vertical profile of amip-4xCO2-spinup − amip anomalous total temperature tendency averaged over the first 17 days of the spinup experiment in the WAM (solid) and NAF (dashed) regions. (b) Vertical profile of amip-4xCO2-spinup − amip anomalous temperature tendency increments averaged over the first 17 days of the spinup experiment in the WAM region. "Other" refers to the sum of boundary layer processes, stratiform precipitation, diffusion, and energy correction, all of which are generally small.

poorly informed. To address this uncertainty, AGCM experiments can be used to simplify the response to increased CO_2 by isolating different aspects of the full coupled model response. In agreement with previous studies, such a decomposition reveals that the direct radiative effect causes an increase in WAM precipitation while the impact of warming SSTs causes a decrease in precipitation. This method of simplifying the response to increased levels of CO_2 can help improve understanding of the processes causing precipitation changes.

Despite the increase in WAM precipitation in response to the direct radiative effect being a well-established result, the underlying mechanism behind this change is poorly understood. Chadwick et al. (2019) suggested a mechanism by which enhanced warming over the Sahara drives a stronger monsoonal flow and an increase in precipitation. However, neither the cause of the enhanced warming nor the link between the temperature changes and the precipitation has been fully established.

Here a single model analysis investigating the equilibrium and spinup response to the direct radiative effect has been performed in order to improve understanding of the mechanism behind the associated precipitation changes.

a. Equilibrium response to the direct radiative effect

In response to the direct radiative effect, the WAM precipitation increases due to a reduction in dry air advection into the monsoon rainband at midlevels resulting from a northward shift and a weakening of the SMC, caused by changes in temperature over North Africa and the Sahel.

Shekhar and Boos (2017) previously illustrated a similar relationship between precipitation and a weakening of the shallow circulation using reanalysis and observational data on interannual time scales. They demonstrated that Sahel precipitation was well correlated with a northward shift and a weakening of the shallow circulation. The results of this paper demonstrate that that the anomalies in temperature, humidity and circulation identified by Shekhar and Boos (2017) as being typical of a wet Sahel year, and a northward shift and a weakening in the SMC, are also seen in response to the direct radiative effect.

Although a strong relationship between precipitation and the changes in the SMC has been demonstrated, it is still not clear exactly why the changes in temperature lead to a weakening of the SMC. This question is beyond the scope of this paper and could be the topic of further work.

b. Spinup response to the direct radiative effect

Changes in the SMC are associated with atmospheric and surface warming patterns over North Africa. In response to the direct radiative effect, a large-scale atmospheric warming pattern, whereby North Africa warms more than the monsoon region, leads to a northward shift in the Saharan heat low. Precipitation changes in the Sahel lead to local changes in surface heat fluxes, with an increase in latent heat flux and a decrease in sensible heat flux. This acts to cool the atmosphere and helps to reinforce the large-scale atmospheric temperature gradients that form over North Africa. It is shown that the soil moisture feedback in the Sahel plays a key role in determining low-level circulation change and the location of the intertropical discontinuity.

Investigating the large-scale warming patterns over North Africa, Chadwick et al. (2019) suggested that enhanced warming over the Sahara occurs due to differing availability of moisture, allowing latent heating adjustments to limit the warming in moist regions but not in dry regions. Merlis (2015) investigated differential heating in response to increased CO_2, with cloud and water vapor masking causing more heating in drier subsidence regions compared to moist convective regions with high cloud. The results of this analysis suggest that the warming patterns seen in response to the direct radiative effect occur not merely due to differential heating

patterns, but also because of differing levels of constraint on atmospheric temperature that apply in different regions.

It is shown by analyzing temperature tendency increments that the differential warming over North Africa cannot be attributed solely to one process causing more warming in one region compared to another, and instead it is a balance of many different terms that leads to the warming patterns seen. Investigating the relationship between the warming due to model physics and warming due to advection, it is shown that over the WAM region, the two terms are strongly anticorrelated, indicating that any warming that occurs due to model physics is effectively and efficiently advected away (and vice versa). In contrast, over the NAF region, this relationship is not seen and the correlation between the model physics term and the advection term is much weaker. It is suggested that this different response occurs due to differing levels of constraint applied to atmospheric temperature by CQE theory and the WTG approximation. Since the WAM region is a convective region and is closer to the equator compared to the NAF region, the column temperature will be set by the MSE below the cloud base (the change in which is small) and constrained to warm at a similar rate to the rest of the tropics. In contrast, this constraint does not apply as strongly over the NAF region, since it is not a convective region and is farther from the equator compared to the WAM region. Therefore, increased radiative heating under increased CO_2 concentrations is able to warm the NAF region more than the WAM region. This argument can be extended to characterize tropical ascent and subsidence regions in general in response to direct CO_2 radiative forcing. Regions of subsidence in the Northern Hemisphere tropics demonstrate a similar response to the NAF region, and regions of ascent demonstrate a similar response to the WAM region.

It is also suggested that changes in near-surface temperature and humidity in the WAM region are small due to the monsoon inflow at low levels originating over the ocean and SSTs remaining unchanged between the amip and amip-4xCO2 experiments.

c. Future work

The results presented in this paper give useful insight into the mechanisms and processes that lead to the WAM precipitation response to the direct radiative effect. However, some gaps in our current understanding still remain. The relationship between warming patterns over North Africa and circulation strength of the SMC is not yet fully understood, and the extent to which SSTs act to constrain low-level temperatures in the WAM region has not been investigated. It is also noted that for this analysis only the month of August has been analyzed (due to limitations of the data used). Further investigation into changes during other months could help further this work, and preliminary analysis of CMIP6 models would suggest that a similar response is seen in other months during the monsoon season too.

A key motivation of this research was to address the uncertainty in WAM precipitation change. The understanding gained from this research regarding the mechanisms driving WAM precipitation change could aid investigation into how this mechanism differs in different models, thus improving our understanding of the uncertainty in WAM precipitation projections. This analysis could also be extended to investigate whether similar responses to the direct radiative effect are seen in other monsoon regions and whether the mechanisms affecting the WAM can be identified elsewhere. Another point of interest would be to investigate whether the processes identified here also act in the opposite sense to produce the precipitation decrease caused by SST warming, or whether in that case a different mechanism is responsible for the precipitation changes. Once this is established, the response of the coupled GCMs could be investigated to see how the two responses to the direct radiative effect and SST warming interact.

Acknowledgments. Mat Collins and F. Hugo Lambert were supported by NERC NE/S004645/1. Harry Mutton was supported by a PhD scholarship from the University of Exeter. Ruth Geen was supported by the U.K.-China Research and Innovation Partnership Fund, through the Met Office Climate Science for Service Partnership (CSSP) China, as part of the Newton Fund. Chris Taylor was supported by the African Monsoon Multidisciplinary Analysis-2050 project (Grant NE/M020428/1). The authors thank the three anonymous reviewers who helped improve the manuscript through their useful comments and suggestions.

Data availability statement. GPCP data are available online and can be downloaded from https://psl.noaa.gov/data/gridded/data.gpcp.html. ERA5 data are available online and can be downloaded from https://cds.climate.copernicus.eu/cdsapp#!/dataset/reanalysis-era5-pressure-levels-monthly-means?tab=form. CMIP6 data were accessed from the ESGF CEDA data node https://esgf-index1.ceda.ac.uk/search/cmip6-ceda/. Data from the HadGEM2-A spinup experiments are archived at the Met Office and available from the authors on request for research purposes.

APPENDIX

Definition of Key Quantities

a. Mass-weighted vertical average

A mass-weighted vertical average has been calculated as

$$\text{mass weighted vertical average} = \int_{p_b}^{p_a} x\,dp/(p_a - p_b), \tag{A1}$$

where x represents the relevant variable being integrated (e.g., temperature), and p_a and p_b represent the top and bottom pressure limits of the integral.

b. Moist static energy

Moist static energy (MSE) has been calculated as

$$\text{MSE} = gZ_g + L_v q + c_p T, \tag{A2}$$

where g is the acceleration due to gravity, Z_g is the geopotential height, L_v is the latent heat of vaporization, q is the specific humidity, c_p is the specific heat capacity at constant pressure, and T is the air temperature.

c. Horizontal divergences

Horizontal divergence of winds and horizontal divergence of moisture transport has been calculated as

$$\text{horizontal divergence of winds} = \nabla_h \cdot \mathbf{V}, \tag{A3}$$

$$\text{horizontal divergence of moisture transport} = \nabla_h \cdot q\mathbf{V}, \tag{A4}$$

where $\mathbf{V}$ is the wind, and ∇_h is the horizontal divergence operator. The change in horizontal divergence of moisture transport between amip and amip-4xCO2 has been decomposed into dynamic and thermodynamic components (Endo and Kitoh 2014):

$$\Delta_{\text{Dynamic}}(\nabla_h \cdot q\mathbf{V}) = \nabla_h \cdot (q_A \Delta\mathbf{V}), \tag{A5}$$

$$\Delta_{\text{Thermodynamic}}(\nabla_h \cdot q\mathbf{V}) = \nabla_h \cdot (\mathbf{V}_A \Delta q), \tag{A6}$$

where subscripts A refer to the amip experiment and Δ refers to the difference between the amip-4xCO2 and amip experiments.

d. Low-level atmospheric thickness

As defined by Lavaysse et al. (2009) and Shekhar and Boos (2017), low-level atmospheric thickness (LLAT) has been calculated as

$$\text{LLAT} = Z_g(700\ \text{hPa}) - Z_g(925\ \text{hPa}), \tag{A7}$$

where $Z_g(x)$ is the geopotential height at pressure x.

REFERENCES

Akinsanola, A. A., and W. Zhou, 2020: Understanding the variability of West African summer monsoon rainfall: Contrasting tropospheric features and monsoon index. *Atmosphere*, **11**, 309, https://doi.org/10.3390/atmos11030309.

Barros, V. R., and Coauthors, 2015: *Climate Change 2014: Impacts, Adaptation, and Vulnerability. Part B: Regional Aspects.* Cambridge University Press, 688 pp.

Biasutti, M., 2019: Rainfall trends in the African Sahel: Characteristics, processes, and causes. *Wiley Interdiscip. Rev.: Climate Change*, **10**, e591, https://doi.org/10.1002/wcc.591.

Bony, S., G. Bellon, D. Klocke, S. Sherwood, S. Fermepin, and S. Denvil, 2013: Robust direct effect of carbon dioxide on tropical circulation and regional precipitation. *Nat. Geosci.*, **6**, 447–451, https://doi.org/10.1038/ngeo1799.

Byrne, M. P., and P. A. O'Gorman, 2016: Understanding decreases in land relative humidity with global warming: Conceptual model and GCM simulations. *J. Climate*, **29**, 9045–9061, https://doi.org/10.1175/JCLI-D-16-0351.1.

Chadwick, R., P. Good, and K. Willett, 2016: A simple moisture advection model of specific humidity change over land in response to SST warming. *J. Climate*, **29**, 7613–7632, https://doi.org/10.1175/JCLI-D-16-0241.1.

——, H. Douville, and C. Skinner, 2017: Timeslice experiments for understanding regional climate projections: Applications to the tropical hydrological cycle and European winter circulation. *Climate Dyn.*, **49**, 3011–3029, https://doi.org/10.1007/s00382-016-3488-6.

——, D. Ackerley, T. Ogura, and D. Dommenget, 2019: Separating the influences of land warming, the direct CO_2 effect, the plant physiological effect, and SST warming on regional precipitation changes. *J. Geophys. Res. Atmos.*, **124**, 624–640, https://doi.org/10.1029/2018JD029423.

Chauvin, F., R. Roehrig, and J. P. Lafore, 2010: Intraseasonal variability of the Saharan heat low and its link with midlatitudes. *J. Climate*, **23**, 2544–2561, https://doi.org/10.1175/2010JCLI3093.1.

Cook, K., and E. Vizy, 2019: Contemporary climate change of the African monsoon systems. *Curr. Climate Change Rep.*, **5**, 145–159, https://doi.org/10.1007/s40641-019-00130-1.

Emanuel, K. A., J. D. Neelin, and C. Bretherton, 1994: On large-scale circulations in convecting atmospheres. *Quart. J. Roy. Meteor. Soc.*, **120**, 1111–1143, https://doi.org/10.1002/qj.49712051902.

Endo, H., and A. Kitoh, 2014: Thermodynamic and dynamic effects on regional monsoon rainfall changes in a warmer climate. *Geophys. Res. Lett.*, **41**, 1704–1710, https://doi.org/10.1002/2013GL059158.

Gaetani, M., B. Fontaine, P. Roucou, and M. Baldi, 2010: Influence of the Mediterranean Sea on the West African monsoon: Intraseasonal variability in numerical simulations. *J. Geophys. Res.*, **115**, D24115, https://doi.org/10.1029/2010JD014436.

——, C. Flamant, S. Bastin, S. Janicot, C. Lavaysse, F. Hourdin, P. Braconnot, and S. Bony, 2017: West African monsoon dynamics and precipitation: The competition between global SST warming and CO_2 increase in CMIP5 idealized simulations. *Climate Dyn.*, **48**, 1353–1373, https://doi.org/10.1007/s00382-016-3146-z.

Geen, R., S. Bordoni, D. S. Battisti, and K. Hui, 2020: Monsoons, ITCZs and the concept of the global monsoon. *Rev. Geophys.*, **58**, e2020RG000700, https://doi.org/10.1029/2020RG000700.

Giannini, A., R. Saravanan, and P. Chang, 2003: Oceanic forcing of Sahel rainfall on interannual to interdecadal time scales. *Science*, **302**, 1027–1030, https://doi.org/10.1126/science.1089357.

Lambert, F. H., M. J. Webb, and M. M. Joshi, 2011: The relationship between land–ocean surface temperature contrast and radiative forcing. *J. Climate*, **24**, 3239–3256, https://doi.org/10.1175/2011JCLI3893.1.

Lavaysse, C., C. Flamant, S. Janicot, D. J. Parker, J.-P. Lafore, B. Sultan, and J. Pelon, 2009: Seasonal evolution of the West African heat low: A climatological perspective. *Climate Dyn.*, **33**, 313–330, https://doi.org/10.1007/s00382-009-0553-4.

——, J. P. Chaboureau, and C. Flamant, 2011: Dust impact on the West African heat low in summertime. *Quart. J. Roy. Meteor. Soc.*, **137**, 1227–1240, https://doi.org/10.1002/qj.844.

Lohou, F., and Coauthors, 2014: Surface response to rain events throughout the West African monsoon. *Atmos. Chem. Phys.*, **14**, 3883–3898, https://doi.org/10.5194/acp-14-3883-2014.

Losada, T., B. Rodriguez-Fonseca, S. Janicot, S. Gervois, F. Chauvin, and P. Ruti, 2010: A multi model approach to the Atlantic equatorial mode: Impact on the West African monsoon. *Climate Dyn.*, **35**, 29–43, https://doi.org/10.1007/s00382-009-0625-5.

Martin, G. M., and Coauthors, 2011: The HadGEM2 family of Met Office Unified Model climate configurations. *Geosci. Model Dev.*, **4**, 723–757, https://doi.org/10.5194/gmd-4-723-2011.

Merlis, T., 2015: Direct weakening of tropical circulations from masked CO_2 radiative forcing. *Proc. Natl. Acad. Sci. USA*, **112**, 13 167–13 171, https://doi.org/10.1073/pnas.1508268112.

Muller, C. J., and P. A. O'Gorman, 2011: An energetic perspective on the regional response of precipitation to climate change. *Nat. Climate Change*, **1**, 266–271, https://doi.org/10.1038/nclimate1169.

Nie, J., W. R. Boos, and Z. Kuang, 2010: Observational evaluation of a convective quasi equilibrium view of monsoons. *J. Climate*, **23**, 4416–4428, https://doi.org/10.1175/2010JCLI3505.1.

Privé, N. C., and R. A. Plumb, 2007: Monsoon dynamics with interactive forcing. Part I: Axisymmetric studies. *J. Atmos. Sci.*, **64**, 1417–1430, https://doi.org/10.1175/JAS3916.1.

Raj, J., H. Bangalath, and G. Stenchikov, 2019: West African monsoon: Current state and future projections in a high-resolution AGCM. *Climate Dyn.*, **52**, 6441–6461, https://doi.org/10.1007/s00382-018-4522-7.

Rowell, D. P., 2001: Teleconnections between the tropical Pacific and the Sahel. *Quart. J. Roy. Meteor. Soc.*, **127**, 1683–1706, https://doi.org/10.1002/qj.49712757512.

Shekhar, R., and W. Boos, 2016: Improving energy-based estimates of monsoon location in the presence of proximal deserts. *J. Climate*, **29**, 4741–4761, https://doi.org/10.1175/JCLI-D-15-0747.1.

——, and ——, 2017: Weakening and shifting of the Saharan shallow meridional circulation during wet years of the West African monsoon. *J. Climate*, **30**, 7399–7422, https://doi.org/10.1175/JCLI-D-16-0696.1.

Skinner, C. B., M. Ashfaq, and N. S. Diffenbaugh, 2012: Influence of twenty-first-century atmospheric and sea surface temperature forcing on West African climate. *J. Climate*, **25**, 527–542, https://doi.org/10.1175/2011JCLI4183.1.

Sobel, A. H., J. Nilsson, and M. L. Polvani, 2001: The weak temperature gradient approximation and balanced tropical moisture waves. *J. Atmos. Sci.*, **58**, 3650–3665, https://doi.org/10.1175/1520-0469(2001)058<3650:TWTGAA>2.0.CO;2.

Todd, A., 2018: Understanding future changes in tropical rainfall and its variability. Ph.D. thesis, University of Exeter, 243 pp.

Wang, B., and Q. Ding, 2006: Changes in global monsoon precipitation over the past 56 years. *Geophys. Res. Lett.*, **33**, L06711, https://doi.org/10.1029/2005GL025347.

——, and Coauthors, 2020: Monsoons climate change assessment. *Bull. Amer. Meteor. Soc.*, **102**, E1–E19, https://doi.org/10.1175/BAMS-D-19-0335.1.

Xia, Y., and Y. Huang, 2017: Differential radiative heating drives tropical atmospheric circulation weakening. *Geophys. Res. Lett.*, **44**, 592–600, https://doi.org/10.1002/2017GL075678.

Yang, Q., A. Majda, and M. Moncrieff, 2019: Upscale impact of mesoscale convective systems and its parameterization in an idealized GCM for an MJO analog above the equator. *J. Atmos. Sci.*, **76**, 865–892, https://doi.org/10.1175/JAS-D-18-0260.1.

Zeng, N., J. D. Neelin, K. M. Lau, and C. J. Tucker, 1999: Enhancement of interdecadal climate variability in the Sahel by vegetation interaction. *Science*, **286**, 1537–1540, https://doi.org/10.1126/science.286.5444.1537.

Zhou, W., and S.-P. Xie, 2018: A hierarchy of idealized monsoons in an intermediate GCM. *J. Climate*, **31**, 9021–9036, https://doi.org/10.1175/JCLI-D-18-0084.1.